A Modular Mechatronic Device for Arm Stiffness Estimation in Human–Robot Interaction

L. Masia, *Member, IEEE*, and V. Squeri

***Abstract*—Measuring human arm stiffness in robot interaction is a crucial topic in both neuroscience and the related learning process during skill acquisition and functional recovery in neurological subjects. However, it is a complex and time-consuming procedure often requiring a computational burden which prevents from an online estimation of the data. Most systems described in the previous literature uses robotic manipulandum to estimate limb stiffness by perturbing the arm across different directions over multiple trials and acquiring the corresponding restoring forces. The proposed method is still robust and accurate, although with rather strong limitations in terms of speed and acquisition bandwidth. For this reason, we designed a mechatronic device able to carry out endpoint stiffness estimation within in a single trial. The proposed system can be operated in a stand-alone configuration or can be plugged in a robotic manipulandum, allowing us to perform the measurement during a posture maintaining task in contact with the robotic counterpart. This paper describes the mechanism and the design, testing the device in different experimental contexts, using a customized test bench to characterize the potentials and the limits of the proposed architecture. Furthermore, we tested the system on human subjects to obtain a reliable bidimensional estimation of arm stiffness when it is plugged in a robotic device. Results are reported and discussed in detail highlighting the limitations and the advantages of using the proposed solution.**

***Index Terms*—Endpoint stiffness, mechatronic device, planar manipulandum, rotary mechanism.**

I. Introduction

A. Background

MOST of the activity we perform using our hands involves interaction with external environment and while manipulating objects, stability is preserved by means of modulation of muscular activity which is controlled by the central nervous system (CNS). Although many tasks are inherently unstable [1], the CNS is able to adapt and counteract to a wide variety of dynamics and the related mechanism behind force regulation is a crucial topic for several disciplines ranging from neurophysiology of motor learning and motor adaptation to robotics and control engineering: potential applications are directly related to technological aspects such as human–robot interaction, rehabilitation and control for robots able to safely interact in a collaborative scenario with a human counterpart [2] in medical robotics and teleoperation [3], [4]. Performance and safety are strictly dependent on haptic stability when the user is physically coupled with the hardware and manipulates the environment [5], [6]. A fast estimation of the mechanical properties of muscular mechanical impedance would be a crucial step to adequately control a robotic system at interface with the human operator. Modulation of the muscular impedance for stability preservation [7] is regulated via changes in muscle activation [8], [9] as the result of the interaction between agonist and antagonist muscular fibers concurrent on each joint; the agonist/antagonist modulation in multijoint movements is characterized by an inherent spring-like properties of muscles [10], while inertial and viscosity of muscles are primarily related to limb configuration and intrinsic features of the muscle fibers, respectively [11]. Stiffness is therefore the principal contribution in impedance modulation [12], steered by the CNS by tuning the activation levels of agonist and antagonist muscles.

B. Previous Methods for Multijoint Stiffness Estimation

The pioneering technique for arm stiffness estimation was based on the acquisition of muscular restoring force in response to a series of separate spatial perturbations across different directions [13] by means of a planar robotic interface. It was found that the endpoint stiffness of the human arm in the horizontal plane is characterized by a directional anisotropy depending on limb geometry and muscular activation levels. Robot generated displacements have been used to estimate stiffness during multijoint movements [14]–[17] and successive experiments [18]–[20] strengthened the robustness of the technique by implementing an adaptive algorithm able to modulate the robot control depending on a prediction of the unperturbed trajectory. Bennet *et al*. [21], [22] and Lacquaniti *et al*. [23] used actuated system to generate stochastic perturbations during voluntary cyclic motion for measuring the resulting time-varying muscular stiffness. A different approach was used by Perreault *et al*. [24] who proposed a stochastic method based on a time/frequency-domain closed-loop multiple-input, multiple-output system identification in a postural task. This approach was introduced in order to overcome the limitations of the previous studies based on multidirectional displacements: in fact, estimates of steady-state stiffness, using directional displacements or force perturbations, require that the subjects "not to intervene" in response to the changes in endpoint position for intervals several times longer than stretch reflex [25] or even voluntary reaction times, ignoring the much larger dynamic components that can arise consequently to a transient external disturbance [26]. Despite all

Manuscript received March 25, 2014; revised July 27, 2014; accepted September 8, 2014. Date of publication December 9, 2014; date of current version August 24, 2015. Recommended by Technical Editor N. G. Tsagarakis.

L. Masia is with the School of Mechanical and Aerospace Engineering, Nanyang Technological University, Singapore 639798, Singapore (e-mail: lorenzo.masia@ntu.edu.sg).

V. Squeri is with the Robotics Brain and Cognitive Sciences Department, Fondazione Istituto Italiano di Tecnologia, Genoa 16163, Italy (e-mail: valentina.squeri@iit.it).

This paper has supplementary downloadable material available at http://ieeexplore.ieee.org provided by the authors. The material consists of a video in WMV format. The size of the file is 6 MB. Contact valentina.squeri@iit.it for further questions about this work.

Color versions of one or more of the figures in this paper are available online at http://ieeexplore.ieee.org.

Digital Object Identifier 10.1109/TMECH.2014.2361925

the numerous studies, endpoint stiffness measurement is still a complex operation, due to the implementation burden and variability of the biomechanical conditions which may lead to high inaccuracy of data. Stiffness estimation requires the use of an actuated device to impose perturbations, starting from the hypothesis that both human arm and robotic device behave linearly for small perturbation, but the combined dynamics of the biological and mechanical system is hard to separate and the linearity of a mechanically actuated system is hard to assume in presence of Coulomb friction which plays a prevalent role for low velocity and small motion amplitude [27], [28]. Recent efforts focused on the design of highly backdriveable mechatronic systems [29]–[31], inspired by previous literature where planar 2-D manipulanda, have been extensively used to perturb human arm to extrapolate stiffness information. We would like to introduce a new direction, by proposing a novel actuated mechanism designed for endpoint stiffness evaluation and consisting in a modular device coupled with a force sensor, which can be plugged in the end effector of any planar robotic manipulandum. By using the proposed architecture, the computational burden associated with the controller of the planar manipulator is greatly reduced, and the modular device results independently driven by its own position control scheme, while in the previous works the robotic planar device should be programmed to directionally perturb the human arm, facing several problems related to bandwidth limitations due to the inertial component of the whole mechanical structure. The proposed solution allows employing the manipulandum to generate haptic force field or providing assistance, while the stiffness estimation is performed by the proposed mechatronic device plugged in the end effector and directly in contact with the human arm.

II. Mechanical Design

The mechanical design of the system was inspired by the position perturbation method proposed for the first time by Mussa-Ivaldi *et al*. [13] which is a widely used technique to asses muscular stiffness; the main problem concerning data acquisition was the generation of the multiple displacements for perturbing subject's hand; the low bandwidth of the planar robot allowed to perturb the end effector in only one direction at a time, needing multiple repeated radial perturbations to evaluate stiffness for a same arm posture. The main limitation of this procedure stems in the *a priori* assumption that all the trials are collected in the same condition of muscular activity: although EMG was used to asses that muscular activation was effectively preserved at the same level, the method still does not overcome the intertrial variability, and above all does not allow to evaluate the arm stiffness within a single execution. Therefore, we designed a mechanism characterized by a high motion bandwidth and able to generate different radial directional displacements in a reduced amount of time in order to measure arm restoring forces within a single trial [32]–[35].

The mechanics of the system consists in two main parts:

The measuring module: it is a commercial six-axis force sensor (ATI Gamma, ATI Industrial Automation, NC, USA).

The motion generator: it is a mechanism able to move the force sensor, applying a series of separate directional radial displacements. This motion pattern has multiple phases opportunely chosen in order to have negligible acceleration of the end effector when the restoring force by the human arm is generated by the muscular stiffness, avoiding the contribution of the inertial and viscous components (see Fig. 1). The mechanism is a planetary gearhead with its sun-gear coupled to a main shaft rigidly connected to a minimum jerk profiled *cam* [see Fig. 1(a)]. The *sun* gear is driven by the primary actuator which transmits the motion to the whole system. The planetary gearhead has been designed with a 7:1 reduction ratio; this means that seven rounds of the *cam* (and the *sun*) correspond to one complete rotation of *carrier* which is driven by the rotation of the three *planets* of the planetary gearhead. The *carrier* is equipped with linear bearings which allow the force sensor (in contact with the human hand) to slide in the horizontal plane with a motion imposed by the *cam* profile. The aforementioned perturbations are delivered in order to allow steady-state force responses observation due to the geometry of the *cam* profile; in fact, acquisition of the restoring force due to muscular stiffness, avoiding the contribution of the inertial and damping components, requires to have a time interval during which the subject's hand is in a steady condition after the directional perturbation.

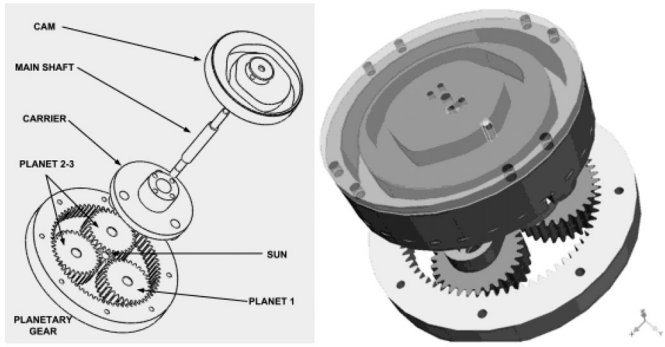

Fig. 1. Assembly of the internal mechanism. (a) Motion-generator is the assembly of a planetary gearhead and a double dwell *cam* mounted on the main shaft which delivers the motion to the whole system driven by an electromechanical actuator. (b) CAD visualization of the motion generator.

Fig. 2 depicts the minimum jerk displacement profile of the *cam*: the interval indicated as *plateau* or *dwell* is the one where restoring force is acquired and subject's hand has no acceleration and velocity. In the proposed mechanical design, to reduce second-order oscillations of the overall mechanical/biomechanical system (arm and robot), a short transition phase minimizing acceleration was achieved by designing the *cam* profile using a sixth-order polynomial law of motion [35]. This is an established design technique, used in *cam* engineering in order to minimize inertial contributions among different members of a mechanism while motion is superimposed. In equation (1), $X(\vartheta)$ is the imposed displacement of the *cam* as function of the *cam* rotation ϑ and C_0–C_6 are the unknown coefficients of the sixth-order polynomial to be determined by imposing zero velocity, acceleration, and jerk at the boundaries of the three phases of rise, fall and dwell, in order to match the

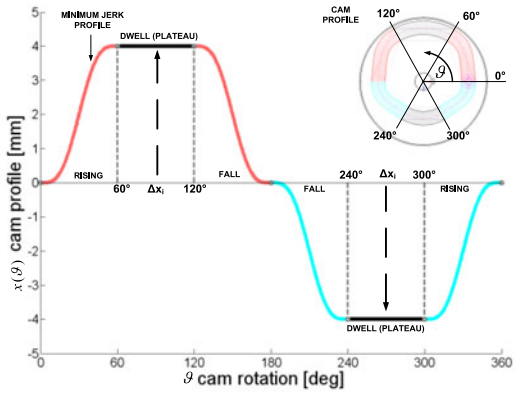

Fig. 2. *cam* profile is profiled by a polynomial displacement allowing a 4 mm motion by a double dwell phase minimizing the acceleration and jerk during risings/fall phases: for each complete rotation, the *cam* delivers two distinct linear 4 mm perturbations in opposite direction.

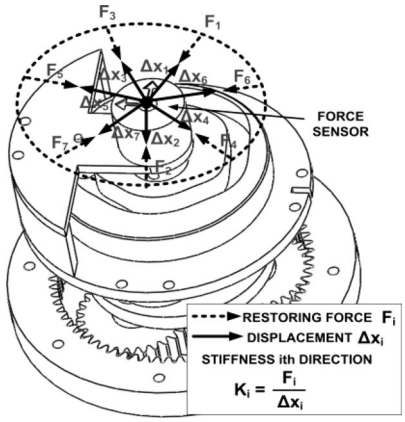

Fig. 3. Mechanical sketch of the assembly. On the top, the force sensor is moved radially and it is rigidly connected to the end effector and the carrier. The mechanism superimposes different radial perturbation ΔXi due to cam rotation over the course of planetary gear motion. Only seven directions are depicted to simplify the sketch.

design specifications for jerk minimization

$$X(\vartheta) = C_0 + C_1 X + C_2 X^2 + \ldots + C_5 X^5 + C_6 X^6$$

$$\left\{ \begin{array}{l} k = [0, 6] \\ \vartheta = k\dfrac{\pi}{3}; \\ \ddot{\vartheta} = \dot{\vartheta} = 0 \end{array} \right\}. \tag{1}$$

Another main requirement was the minimization of the time interval for the multiple motion perturbations: hence, we decided to design a *double dwell cam* which, for each complete rotation ($\vartheta = 360°$), displaces the subject's hand in two directions (see Fig. 2). The *double dwell* profile allows having two perturbations in one complete turn of the *cam* and thus a whole turn of the *carrier* allows perturbing across 14 different radial directions with phases of zero velocity and acceleration, considering the 7:1 reduction ratio of the planetary gear.

For sake of simplicity, the sketch in Fig. 3 depicts only seven directions, corresponding to a 180° rotation of the *carrier*. When the system starts rotating, the *cam* pushes the *sliding carriage* and the *force sensor* in one direction, displacing the subject's hand by a preset amount ΔX_1 that is defined by the geometry of the *cam profile* (in our design is 4 mm). The hand's restoring force F_1 is acquired by the *force sensor*; hence, a directional value of the stiffness K_1 is obtained as the ratio:

$$K_1 = \frac{F_1(\vartheta)}{\Delta X_1(\vartheta)}. \tag{2}$$

While the *cam* rotates, the *carrier* and the *sliding carriage* rotate with a slower angular speed, which is imposed by the *reduction ratio* of the *planetary gear* head (7:1). The remaining arc of the *cam* profile perturbs the hand in the opposite direction shifted with respect to the previous one by the amount of rotation made by the *carrier* and 180° because the *cam* is double-dwell. The hand is now displaced by ΔX_2 and the corresponding reaction force F_2 is acquired by means of the *force sensor*.

The stiffness associated with the new direction will be

$$K_2 = \frac{F_2(\vartheta)}{\Delta X_2(\vartheta)}. \tag{3}$$

Since directional arm stiffness is not isotropic but strongly depends on muscular activation and posture, the two evaluated forces F_1 and F_2 will be different. When the *planetary gear-head* or the *carrier* completes one round, the system will have scanned 14 directions, because 7:1 is the reduction ratio of the *planetary gear* and 14 values of directional stiffness will have been evaluated

$$K_1 = \frac{F_1}{\Delta X_1}; K_2 = \frac{F_2}{\Delta X_2}; \ldots K_{14} = \frac{F_{14}}{\Delta X_{14}}. \tag{4}$$

Using such a designed system, it is possible to estimate multidirectional stiffness in a reduced amount of time; the mechanism allows combining multiple measures in a single execution, avoiding intertrial variability previously mentioned in the experiments using robotic setups and requiring a single trial for each directional measurement.

III. Methods

The device has been tested in three different conditions: 1) using a customized test-bench for directional stiffness simulation; 2) in a stand-alone mode on two human subjects while holding three different arm postures; and 3) coupling the device to a planar manipulandum for stiffness acquisition during posture maintaining tasks across five different arm configurations. In the following section, the characterization of the system will be described to test reliability, accuracy, and bandwidth limitation, and the remaining part of this paper will deal with a preliminary human trials for stiffness estimation.

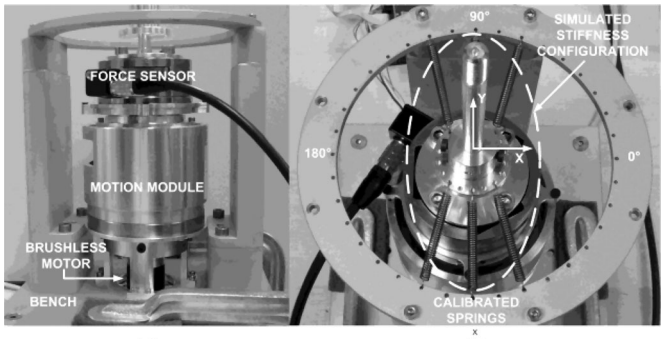

(a) (b)

Fig. 4. Experimental setup for preliminary test and characterization. (a) Overview of the device (motion module and force sensors) connected to the bench. (b) Top view of the test bench used to simulate principal direction of stiffness.

A. Preliminary Characterization of the System by Test Bench

Measuring arm stiffness is not a trivial procedure, remaining focused on biomechanical applications; previous methods suffer from the limitation that a perturbation of the same amplitude, during different trials, applied at different points in the trajectory or in different directions, will receive a restoring force by the hand of different amounts.

This is because limb stiffness is strongly dependent on joint angles, angular velocity, and perturbation direction; the proposed mechanical device has the main goal to measure stiffness without disrupting posture and motion concentrating the time required for stiffness ellipse evaluation within a single measurement. Before testing the device on humans, the system has been characterized by means of a customized setup (see Fig. 4). It consists in a test bench able to simulate different stiffness configurations by multiple springs attached between an external frame and the force sensor of the device which is plugged in. In this way, it has been possible to accurately simulate desired stiffness values and the orientations, by attaching the springs' end points to different machined holes of the supporting frame and spatially configuring them in accurate angular mutual distances. The test is then focused on the capability of the device to precisely detect the orientation of the stiffness ellipse, and its magnitude. It is worth to highlight that knowing (with a good approximation) the springs' stiffness constant, and their mutual angular orientations on the frame, it is possible to evaluate the simulated stiffness ellipse. Observing Fig. 5(a) depicting the working principle of the test bench, the mass *M* connected by springs $k_1, k_2, \ldots, k_n$ is constrained to move on the plane *x–y* as it was the moving part of the proposed device on which the force sensor is mounted. If the mass is displaced from its static equilibrium position O along the *X* direction, the spring K_1 is deformed and consequently applies a restoring force with two components on the *XY* plane [see Fig. 5(b)]:

$$\begin{aligned} F_{1x} &= XK_1\cos^2\theta_1 \\ F_{1y} &= XK_1\cos\theta_1\cos\phi_{11}. \end{aligned} \tag{5}$$

Therefore, if one considers the contribution of all the springs for a displacement in the *X* direction, the overall contribution of the components of the restoring forces in the *XY* plane can be summarized with the following formulas:

$$\begin{aligned} F_{\sum_1^n kx} &= X(K_1\cos^2\theta_1 + \ldots + K_n\cos^2\theta_n) = K_{xx}X \\ F_{\sum_1^n ky} &= X(K_1\cos\theta_1\cos\phi_1 \ldots + K_n\cos\theta_n\cos\phi_n) = K_{yx}X. \end{aligned} \tag{6}$$

In a similar manner if the mass *M* is displaced in the *Y* direction [see Fig. 5(c)], we find the total contribution of the springs acting on the mass *M* as follows:

$$\begin{aligned} F_{1x} &= YK_1\cos^2\phi_1 \\ F_{1y} &= YK_1\cos\theta_1\cos\phi_1 \\ F_{\sum_1^n kx} &= Y(K_1\cos^2\phi_1 \ldots + K_n\cos^2\phi_n) = K_{xy}Y \end{aligned} \tag{7}$$

$$F_{\sum_1^n ky} = Y(K_1\cos\theta_1\cos\phi_1 \ldots + K_n\cos\theta_n\cos\phi_n) = K_{yy}Y. \tag{8}$$

The resulting stiffness can be expressed in matrix form by the static equations between the mass displacement and the restoring forces delivered by the springs after a planar perturbation in a composed *X* and *Y* direction is applied:

$$\begin{bmatrix} F_x \\ F_y \end{bmatrix} = \begin{vmatrix} K_{xx} & K_{xy} \\ K_{yx} & K_{yy} \end{vmatrix} \begin{bmatrix} X \\ Y \end{bmatrix}. \tag{9}$$

The frame depicted in Fig. 5(a) allows generating different stiffness orientations depending on the springs' configurations as represented at the right of Fig. 5: this simple setup provides the possibility to test the device and characterize its capability to discriminate stiffness magnitude and orientation but above all, to find the maximum rotational regime at which the device can still provide an accurate measurement. Table I indicates the speed values at which the system performs the motion of the force sensor in order to estimate stiffness for the chosen springs' configuration: in this paper for sake of space, we will present only the test performed on a vertical stiffness simulation, focusing the attention on the tradeoff between data information and mechanical noise arising at different rotational regimes of the mechanism.

B. Evaluation of Arm Stiffness in Stand-alone Mode

Preliminary test on human subjects has been performed before mounting the device on a robotic planar manipulandum. We designed the cam profile assuming that during the dwell the linear velocity and the acceleration of the arm are close to zero and the inertial and damping contributions during each radial perturbation can be considered negligible respect to the one of the restoring force due to the muscular stiffness. When the arm is perturbed from an equilibrium position, the restoring force results to be non colinear with the direction of the imposed displacement [see Fig. 6(c)]; hence, a specific algorithm will be discussed and used to determine the irrotational components of

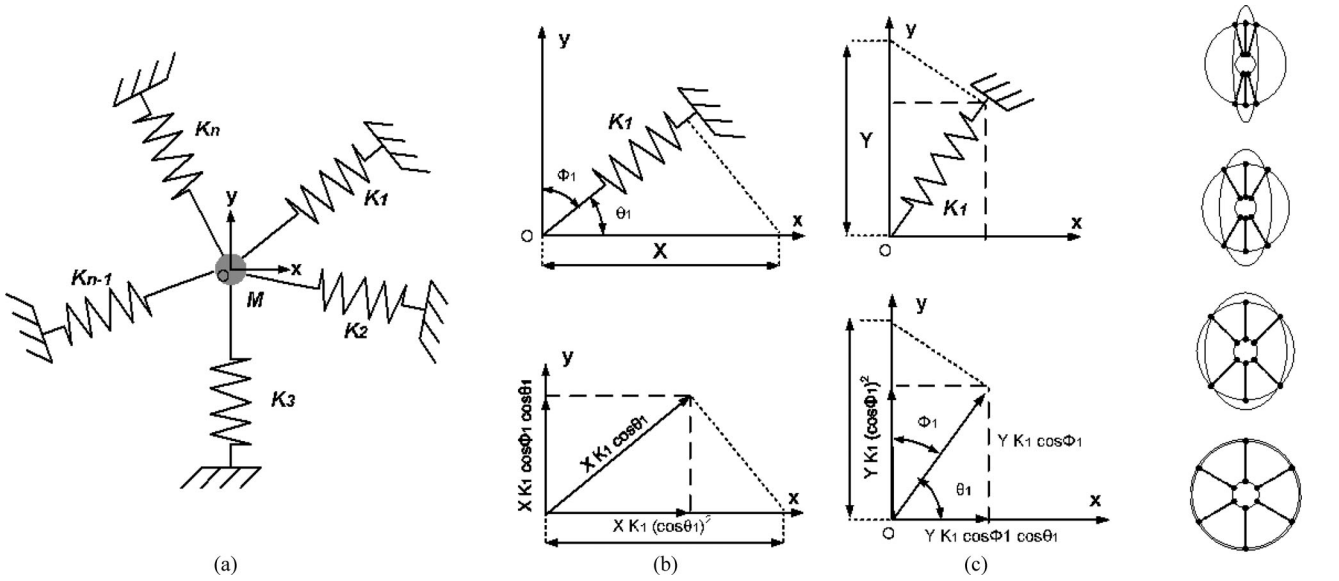

Fig. 5. Top figure: schematic sketch of the working principle of the test bench. (a)–(c) Representation of the test bench and restoring force components provided by the springs. Right figure: different contributions to the generated stiffness ellipse as function of the spring configuration on the external frame.

TABLE I
EXPERIMENTAL CONDITION OF THE CHARACTERIZATION TEST

r/min	Execution time [s]	Principal direction
100	13.47	
300	4.49	
500	2.69	
800	1.83	**90° on the plane *XY* of the force sensor**
1000	1.24	
1500	0.96	
1800	0.82	
2000	0.75	

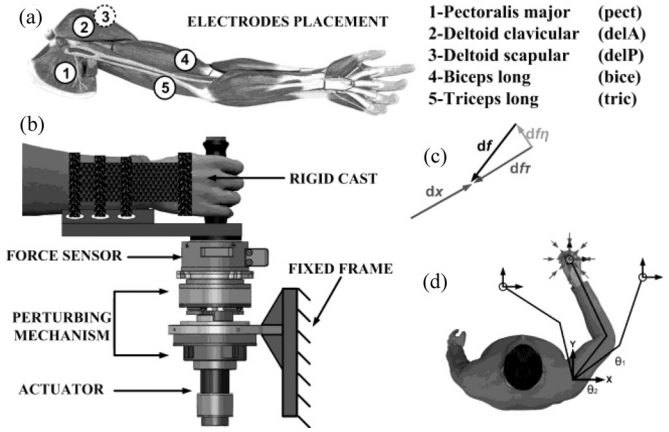

Fig. 6. Setup for experiment on humans. (a) Electrode placements were chosen in order to observe the muscular activity over the trials for stiffness estimation. (b) Cast and handle used to restrain wrist flexion/extension during measurement. (c) Noncolinearity of the restoring forces during human trial. (d) Three different postures were tested in proximal and distal configurations.

the forces and the symmetric stiffness matrix. Endpoint stiffness was estimated using the device firmly attached to a fixed frame and equipped by a handle used to hold the subjects' wrist in the neutral position by means of a rigid cast [see Fig. 6(b)]: in such a way during the measurement only the elbow and the shoulder joints have been perturbed. Subjects seated in front of the device with their right shoulder restrained by a seatbelt in order to avoid trunk movement; they were instructed to grasp the handle of the device and stiffen up the arm; a five channels EMG [see Fig. 6(a)] was used with the purpose of observing the variation of the muscular activity during each trial and providing the subject with a visual feedback (green light appearing on a screen) once contraction level reaches the threshold of 40 $\pm$ 10% of his/her maximum voluntary contraction: it is important to point out that the evaluated stiffness is given by the contributions of both the voluntary cocontraction and the stretch reflex arising in the first 60–100 ms [36], [37] during each single perturbation operated by the cam motion. In most of previous experiments on stiffness quantification, the stretch reflex was considered a component altering the exact estimation of the muscular activation and jeopardizing the final result. Contrarily for robotic applications, we strongly believe that the dynamics of interaction must comprise all the contributions provided by both the stretch reflex and voluntarily control of limb. Furthermore, previous studies confirmed that the reaction by stretch reflex is highly dependent on the level of muscular activity and it reaches its peak (20% of the EMG signal) only in case of maximum voluntary cocontraction [38]–[43] that is why we chose to acquire the restoring force after multidirectional displacements when the muscular activation is not maximal.

C. Arm Stiffness in Posture Maintaining Task

A further experiment consisted in testing the device when is plugged on the end-effector of a planar manipulandum. Four subjects were enrolled in the experiment to evaluate planar stiffness at the hand during posture maintaining task for different

locations of the robot workspace (see Fig. 8), replicating the experiment run by Mussa-Ivaldi *et al*. [13]: subjects were required to let the robot drives their right arm to a specific position and then firmly hold the handle increasing the muscular tone. The choice of letting the robot actively positioning the subjects' hand was dictated by the need of having accurate and repeatable configurations of the arm for the same location in the workspace. For each subject, five different arm configurations were tested (five different stiffness measurements), in three nonconsecutive acquisitions. Prior the experiment, subjects' EMG was recorded for different levels of muscular voluntary contraction: the main purpose was to synchronize the motion of the manipulandum by triggering the stiffness estimation using subject's muscular activations. For each subject and each of the five arm configurations, we measured the EMG signals at rest (no muscular activity), and maximum voluntarily contraction: the subjects were then instructed to contract at about 40 $\pm$ 10% of the maximum value previously measured and visual feedback of the desired muscular activity level was provided by a green color of the cursor identifying the position of the human hand in the robot workspace. A preset level of muscular activity for each of the four participants was requested for activating the device and acquiring the force: the EMG level has been used as trigger signal for the stiffness measurement as described in the following paragraph. Once the planar robot has reached one of the five configurations, the subject was asked to increase the muscle tone of his/her 40 $\pm$ 10% and hold it. Once the required EMG level has been reached, after about 1 s the handle was shacked across seven different radial directions and the stiffness was estimated for the actual locations in the workspace (see Fig. 7, top). In the experimental setup using the robotic device, it is crucial to factor out the specific contributions to the measurement from the robot and the human arm in order to avoid systematic errors in stiffness evaluation.

Since the measuring device is mounted on the end effector of the robot, the amount of displacement imposed during the *cam* rotation will be delivered to both the systems: the subject's arm and the planar robot. In order to decrease the amount of displacement of the planar manipulandum and to limit the oscillations, the robot was operated by an impedance controller ramping up stiffness (2500 N/m) and damping (200 N $\cdot$ s/m) gains once each of the five locations in the workspace has been reached (see Fig. 7, bottom). In this way before starting the stiffness measurement, the manipulandum resulted in a more rigid configuration hence less sensitive to vibrations due to the radial perturbations.

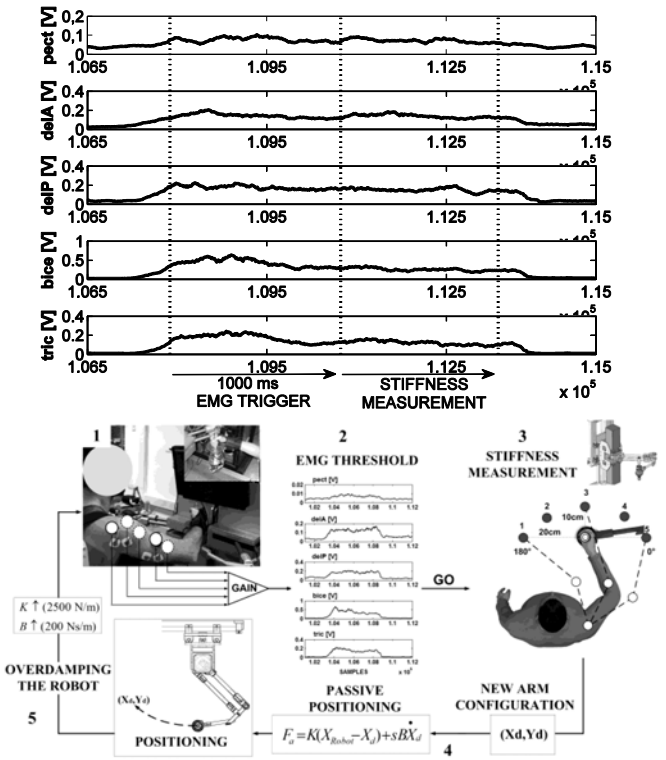

Fig. 7. Top: EMG signal used to trigger the stiffness measurement. Bottom: sequence of the stiffness measurement; (1)–(2): the subjects increase the muscular activity holding the position and triggering the stiffness measurement (3). After the acquisition, the planar manipulandum passively moves (4) the subject's arm in a new configuration (X_d, Y_d) and hold the position increasing the stiffness and damping in the controller (5) in order to limit the oscillation during the next radial perturbations before the new measurement.

IV. Results

A. Test Bench for Directional Stiffness Evaluation

The device was tested at different rotational speeds: Fig. 8(a) depicts the absolute value of the restoring force by the springs during the carrier rotation and the radial displacements; the *cam* perturbs the springs seven times corresponding to a 180° of carrier rotation; by limiting the maximum rotation of the carrier, the execution time is decreased, but still preserving an amount of data sufficient to estimate the stiffness ellipse. The intervals of interest are the *dwells* of the *cam* where the springs are stretched by 4 mm radial displacements and are indicated in Fig. 8(a) as gray square markers.

In this phase, the acceleration superimposed by the *cam* profile to the springs is null and the amount of acquired force is only to be intended as the contribution of the restoring action delivered by the springs' stiffness. The force is acquired and correlated with the actual displacement and direction in order to obtain the stiffness ellipse [see Fig. 8(b)]. For motions around an equilibrium position, the direction of the vectors of the restoring force *F* and of the displacement imposed by the *cam* profile $\Delta X(dx, dy)$ are related by the following equations:

$$\begin{aligned} F_X &= (f_{1x}, ..., f_{nx})\,; F_Y = (f_{1y}, ..., f_{ny}) \\ dx &= (dx_{1x}, ..., dx_{nx})\,; dy = (dx_{1y}, ..., dx_{ny}) \quad (10.a) \\ dF_x &= -K_{xx} \cdot dx - K_{xy} \cdot dy \\ dF_y &= -K_{yx} \cdot dx - K_{yy} \cdot dy \\ \overline{F} &= -K \cdot \overline{\Delta S}. \quad (10.b) \end{aligned}$$

In purely elastic systems, the off-diagonal terms K_{xy} and K_{yx} should be equal in magnitude and this comes from the reason that if a potential function can be defined, then the resulting stiffness matrix is symmetrical. In the test bench, the presence of small misalignments between the reference frame and the

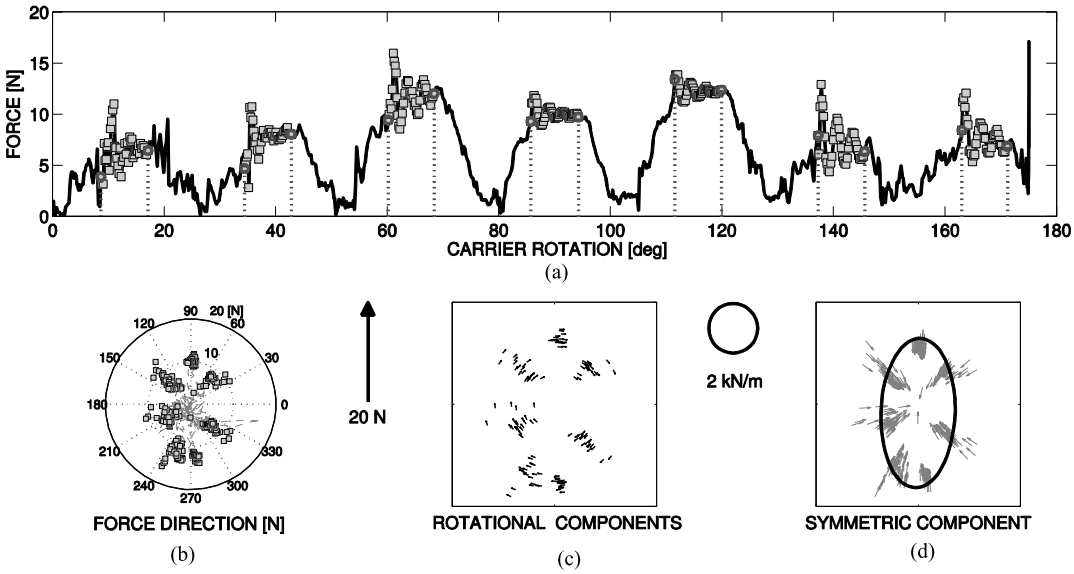

Fig. 8. Stiffness measurement. (A) Plot of the absolute value of the restoring force during *cam* action (rising-dwell-fall = 800 r/min) in function of the angular orientation of the carrier. The black trace corresponds to the value of the directional force. Intervals of interest for stiffness evaluation are highlighted by vertical dotted lines indicating the dwell phases of the *cam* and restoring forces used to run the regression algorithm are indicated as gray-squared markers. (B) Visualization of restoring forces in the dwell phase over the different directions of perturbation executed in one single trial. (C) Rotational components of the force are depicted and evaluated by decomposing the stiffness matrix in symmetric and antisymmetric tensor. (D) Symmetric conservative components of the force and related stiffness ellipse.

force sensor may introduce components of the restoring force which are not colinear with the radial displacements direction. Hence, for the analysis, the stiffness estimation was decomposed in symmetric or irrotational (K_S) and antisymmetric or rotational (K_A) matrixes in order to separate the conservative and nonconservative components of the force field:

$$\begin{aligned} K &= K_S + K_A \\ K_S &= \begin{bmatrix} K_{xx} & 1/2(K_{xy}+K_{yx}) \\ 1/2(K_{xy}+K_{yx}) & K_{yy} \end{bmatrix} \\ K_S &= \begin{bmatrix} 0 & 1/2(K_{xy}-K_{yx}) \\ 1/2(K_{xy}-K_{yx}) & 0 \end{bmatrix}. \end{aligned} \tag{11}$$

After the symmetric stiffness tensor has been evaluated, the ellipse was represented by finding the eigenvalues and eigenvectors. Larger and smaller eigenvalues are the forces exerted along major and minor axes of the stiffness ellipse, and the orientation of the ellipse is obtained by the angle (θ) between the major eigenvector and the horizontal x axis of the plane on which the measurement is performed:

$$\begin{aligned} K_S &= \begin{bmatrix} k_1 & k_2 \\ k_2 & k_3 \end{bmatrix} \\ \lambda_{1,2} &= \frac{1}{2}\left[(k_1+k_3) \pm \sqrt{(k_1+k_3)^2 + 4(k_2^2 - k_3 k_1)}\right] \\ R &= \frac{\lambda_1}{\lambda_2}; \vartheta = \operatorname{arctg}\left(\frac{(\lambda_2 - k_1)}{k_2}\right) = \operatorname{arctg}\left(\frac{k_2}{(\lambda_2 - k_1)}\right) \end{aligned} \tag{12}$$

where λ, R, and θ are, respectively, the eigenvalues, aspect ratio, and orientation of the stiffness ellipse. Fig. 8(c) and (d) shows the antisymmetric rotational component of the force and the symmetric ones, respectively; the stiffness ellipse is generated by considering only the conservative (irrotational) forces and correlating them with directional displacements. Before testing the device on humans, we find out the minimum time execution for which the device can still accurately estimate the stiffness ellipse. Previous works [18] considered an 8–10 mm single 300 ms directional perturbation at which arm steady-state force response was acquired and repeated across multiple directions; we chose to space *seven* different directions in the shortest possible time without separating the trials, trying to obtain a good tradeoff between accuracy, repeatability, and rejection of noise due to the rotational speed of the *cam*. Fig. 9 depicts the absolute value of the force measurements at different angular speeds of the *cam* as function of angular rotation of the carrier. For high rotational regimes (800–1000–1500–1800–2000 r/min), despite filtering, the force signal is affected by mechanical noise mostly concentrated in correspondence of the dwells, where the inertial contribution of the mechanism due to the high value of accelerations/decelerations causes oscillations. It results that the corresponding stiffness evaluation will be more accurate depending on the efficacy of data filtering: a second-order Butterworth filter was used to clean the force signal from oscillations and mechanical noise during the acquisition for higher speed of the *cam*. From Fig. 10 emerges that the 2-D stiffness evaluation is not acceptable for rotational regimes beyond 1500 r/min; for such high angular speeds of the *cam* (1800 and 2000 r/min), the data used for stiffness evaluation (black thicker lines in the dwells phase from Fig. 9) result jeopardized by mechanical noise, and the experimentally evaluated ellipses do not preserve a comparable

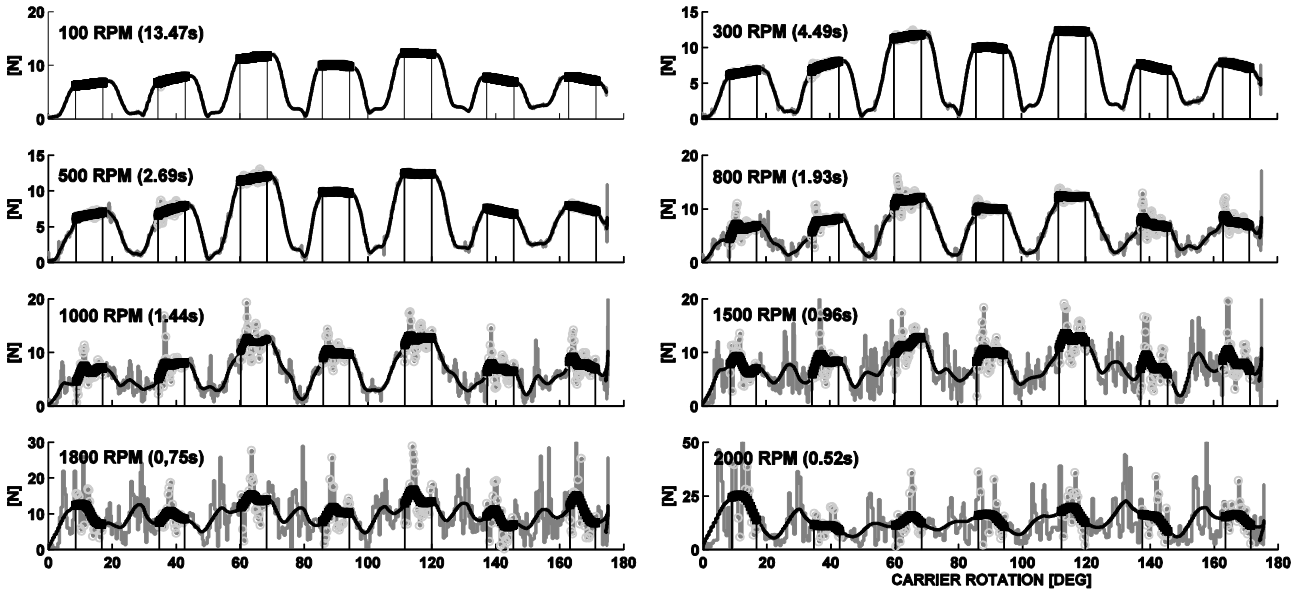

Fig. 9. Measurement of the restoring force at different angular speeds. Force signals raw (gray) and filtered (black) for different trials at different rotational regimes of the main shaft. As clearly shown, increasing the angular speed, mechanical vibrations affect the measurement. Intervals of interest for computation of stiffness are considered those corresponding to the dwell of the cam, and are depicted as thicker black lines.

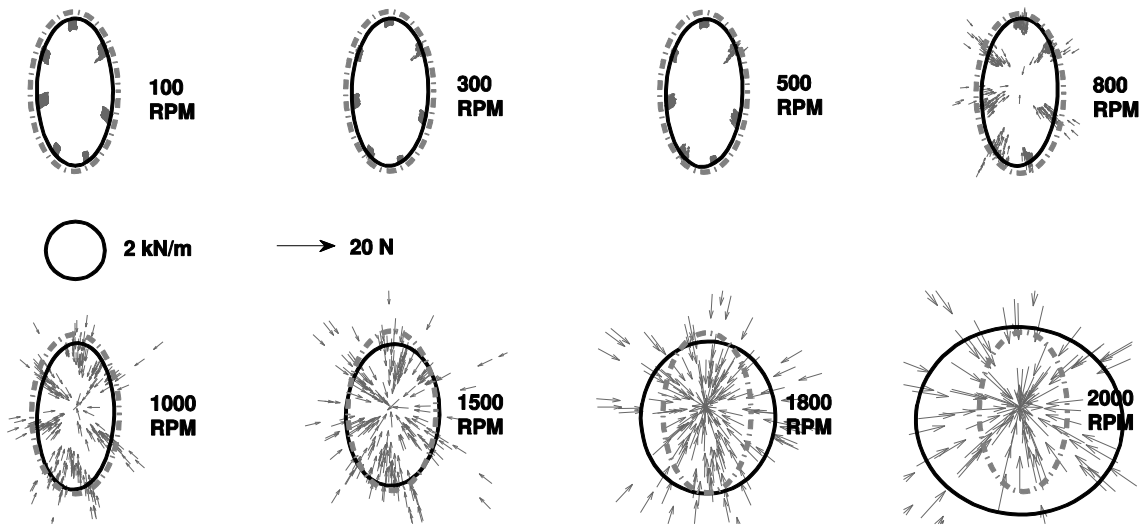

Fig. 10. Measuring at different angular speeds. Visualization of the estimated stiffness ellipses at different rotational regimes. Symmetric conservative components of the forces are depicted as arrows. Dashed gray stiffness ellipses are the theoretical ones simulated by the test bench while the estimated ellipse from force acquisition are depicted in black solid lines.

shape with the theoretical one (gray dotted ellipse in Fig. 10). While for lower rotational regimes (100, 300, 500, 800, 1000, and 1500 r/min), the stiffness ellipses present a good level of accuracy.

B. Human Test in Stand-alone Configuration

For the stand-alone test, trials were recorded on two unimpaired subjects, for three different arm postures at 1500 r/min (960 ms execution time) of the mechanism acquiring the signal at 2.5 kHz sampling frequency, in order to check if the device is able to discriminate the different contributions of the musculoskeletal system and stiffness orientations. Plots of the force signal during a single stiffness measurement is reported in Fig. 11(a); observing the force plot it is possible to identify the seven peaks corresponding to the seven directions of perturbations (*dwells* indicated by the letter "D"). The force signals used for stiffness estimation are delimited by vertical lines, while thick black lines highlight those force peaks corresponding to each single perturbation (about 60 ms duration) where the restoring force by the musculoskeletal system is measured and the *cam* is not transmitting any linear motion to the subject's hand.

Fig. 11(b) shows the five EMG signals acquired during a single trial: the test measurement was initiated 1 s after the contraction and the muscular activity during the whole execution time

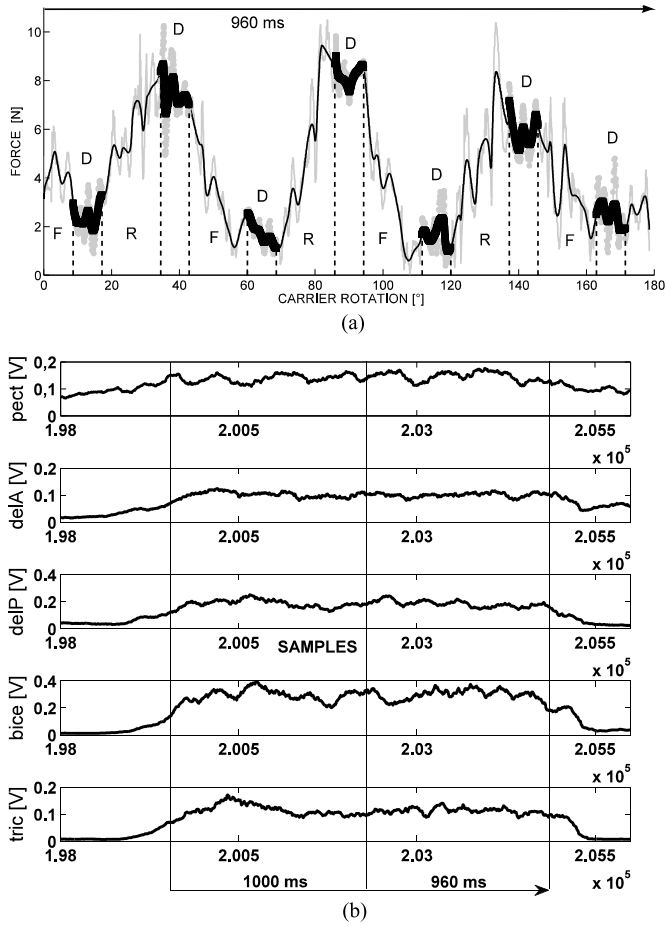

Fig. 11. Single human trial. (a) Plot of force during the directional displacements where F-R-D are the cam phases fall-rise-dwell, respectively. The R and F segment impose motion to the subject's hand depending on rotational speed of the cam and its profile, while the D segment is defined as a no-input motion. The gray and black signals are the raw and filtered force, respectively: thick black intervals are the restoring forces used for stiffness evaluation. (b) EMG signals of the five muscles during the seven radial displacements.

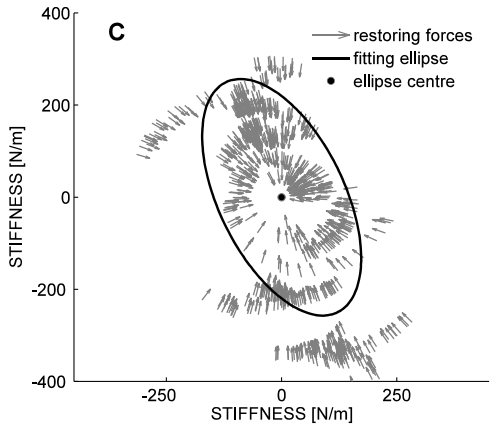

Fig. 12. Representation of the stiffness ellipse and the conservative components of the normalized forces (unitary module). The distance between the tip of each arrow and the center of the ellipse is the force module.

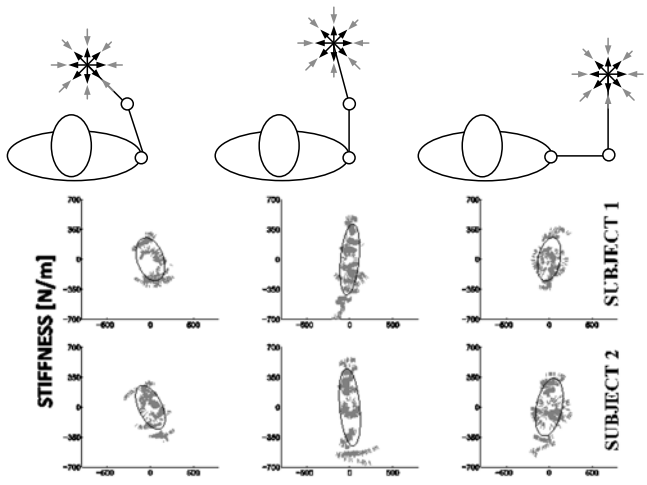

Fig. 13. Stiffness ellipse evaluated in stand-alone mode on two subjects. They were required to hold the handle of the device and maintain the configuration of their arm. Symmetric component of the restoring forces is depicted as gray arrows.

remains almost constant. Reconstructed stiffness ellipse and restoring forces from symmetric stiffness matrix are depicted in Fig. 12 by a black line and small gray arrows, respectively.

Results for the two subjects are shown in Fig. 13 where each stiffness ellipse is obtained for three tested posture of the arm which are indicated at the bottom of the figure by schematic sketches: the three different arm configurations were chosen in order to highlight the change in stiffness ellipse orientation when the subject assume different arm postures. In the graphical representation of the stiffness, the direction of the major axis changes as function of arm configuration, becoming more elongated as the hand location is moved in a more distal position (see Fig. 13 center), while a more isotropic distribution of the stiffness is observable when the hand location is closer to a proximal configuration (see Fig. 13, left and right).

C. Human Test With Planar Manipulator

Despite the manipulandum firmly holds the position as previously explained, the oscillations delivered by the modular device during the measurements inevitably introduce a component of displacement in the kinematic of the planar robot. Hence, to estimate the exact amount of motion of the subject's hand, one needs to accurately separate the two displacement components, respectively, delivered to the subject's arm and the planar robot. Fig. 14(a) shows that before starting the measurement with the stiffness device and the manipulator hold coincident positions in the workspace (indicated as a vertical dotted line); later on each single directional displacement delivered by the *cam* ($\Delta X_{\rm tot}$) is partly delivered to the subject's hand (ΔX_H) and to the planar robot (ΔX_R) [see Fig. 14(b) and (c)]. The amount of displacement transmitted to both the mechanical and biomechanical systems in contact with the modular device is proportional to their compliance [see Fig. 14(d)]: in the ideal case of infinite rigidity by the robot (zero compliance $K_R = \infty$) its motion during the radial perturbation would be zero ($\Delta X_R = 0$) and the total superimposed displacement (*cam* rise or fall) would be entirely transferred to the subject's arm ($\Delta X_H = \Delta X_{\rm tot}$). In a

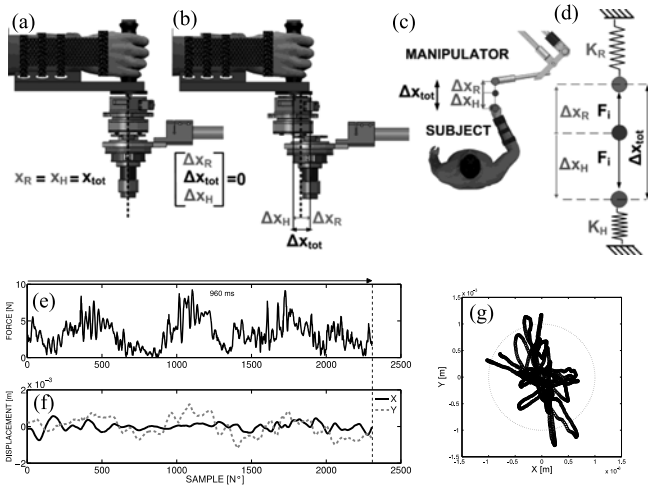

Fig. 14. (a)–(d) Relative motion between the manipulandum and the subject's hand during each of the directional perturbation. (e) Force measurement for the seven directional perturbations. (f) Displacement of the robot end effector in the coordinated axes of the workspace and in the plane (g).

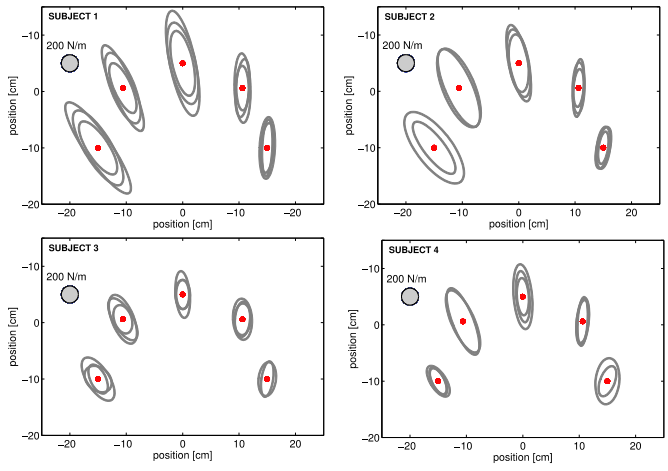

Fig. 15. Stiffness ellipse estimation for four subjects, in five different workspace locations. Subjects were guided passively by the robotic manipulandum and then they were required to increase muscle tone to trigger the device and measuring the restoring forces during the planar multidirectional perturbation.

real scenario, the amount of motion delivered to the subject's hand and the planar robot will be inversely proportional to their respective stiffness as conceptually sketched in Fig. 14(d) and they can be evaluated with a good level of accuracy because 1) the interaction forces [see Fig. 14(e)] and the kinematics [see Fig. 14(f) and (g)] of the planar robot are instantaneously measured in the workspace by the force sensor and the encoders; and 2) the total amount of displacement ($\Delta X_{\rm tot}$) is known from the *cam* geometry. The actual motion imposed by the device to subject's hand is therefore given by the algebraic sum of the motion due to *cam* profile ($\Delta X_{\rm tot}$) and the one of the robotic end effector (ΔX_R) [see Fig. 14(f) and (g)]. By considering the hand's actual displacement $\Delta X_H = \Delta X_{\rm tot} - \Delta X_R$, the regression analysis allows to estimate the stiffness of the arm neglecting the counterpart due to the manipulator as reported in

$$\begin{bmatrix} F_X \\ F_Y \end{bmatrix} = -\begin{bmatrix} K_{XX} & K_{XY} \\ K_{YX} & K_{YY} \end{bmatrix} \begin{bmatrix} (\Delta x_{\rm tot} - \Delta x_R) \\ (\Delta y_{\rm tot} - \Delta x_R) \end{bmatrix}. \quad (13)$$

Results are shown in Fig. 15 where each interpolating ellipse is obtained from a single (960 ms duration) measurement in the different arm postures; as expected the major axis of the ellipse is approximately oriented from the distal to the proximal part of the limb showing also a good level of repeatability that can be observed in the ellipses' orientation in the same workspace location, defined as the inclination of the major axis of the ellipse with the horizontal axis of the robot (see Table II).

To test if the computed angles of the ellipses (θ) were different for the five positions in the workspace, we performed a one way ANOVA (repeated measures) with POSITION as main effect. The main effect for POSITION was highly statistically significant ($F(4, 12) = 17772$, $p < 0.05$) underlining the notion that the means of the five locations were different from each other, with a decreasing θ moving from the left part to the right part of the workspace [see Fig. 16(a) and (b)]. Table III provides the

TABLE II
INCLINATION OF THE STIFFNESS ELLIPSES OF THE SUBJECTS' ARM IN THE FIVE LIMB CONFIGURATION OVER THE WORKSPACE OF THE PLANAR MANIPULANDUM

θ [deg]	1	2	3	4	5
Subject 1	126.1 ± 2.8	115.1 ± 4.6	101.3 ± 3.7	89.3 ± 2.7	86.3 ± 1.3
Subject 2	130.2 ± 3.1	114.6 ± 2.2	103.8 ± 1.0	86.7 ± 3.9	81.9 ± 2.2
Subject 3	123.6 ± 1.3	120.2 ± 1.3	97.7 ± 1.5	86.2 ± 1.8	83.5 ± 0.1
Subject 4	127.4 ± 1.2	114.2 ± 3.4	96.2 ± 2.9	85.5 ± 3.5	76.7 ± 2.4

stiffness values averaged across trials on the same position in the robot workspace: K_M and K_m are referred to the stiffness in the major and minor axes of the interpolated ellipse.

V. DISCUSSION

A. Potentials and Limitations of the Proposed Technology

The importance of measuring the scalar and directional properties of the arm stiffness in motor behavioral studies has been always considered crucial [44]–[46]. The first investigations on dynamics of musculoskeletal systems were performed by applying disturbances of different types during posture and movement on humans and primates, initially by superimposing single degree of freedom displacements and then with multiple DoFs paradigm. Mussa-Ivaldi [13] was the first to use a planar manipulandum for the measurements of the mechanical impedance of the human arm and its representation in terms of stiffness/viscosity/inertial ellipses. Robotic devices of that kind are capable to carry out the estimation of the mechanical stiffness associated with muscular activity because of their backdriveability and they can provide accurate inputs of positional disturbances and measure the correlated restoring forces. On the other hand, this kind of technology is designed in such a way to access a large workspace, comparable to the human range of motion, and thus it is characterized by a nonnegligible mass and intrinsic

TABLE III
MAJOR AND MINOR AXES OF THE STIFFNESS ELLIPSES OF THE SUBJECTS' ARM IN THE FIVE LIMB CONFIGURATION OVER THE WORKSPACE OF THE PLANAR MANIPULANDUM

$K_M, K_m [N/m]$	1	2	3	4	5
Subject 1	$K_M = 437 \pm 93$ $K_m = 129 \pm 21$	$K_M = 467 \pm 98$ $K_m = 114 \pm 15$	$K_M = 538 \pm 78$ $K_m = 167 \pm 14$	$K_M = 380 \pm 52$ $K_m = 97 \pm 12$	$K_M = 300 \pm 15$ $K_m = 78 \pm 10$
Subject 2	$K_M = 398 \pm 77$ $K_m = 128 \pm 45$	$K_M = 423 \pm 35$ $K_m = 174 \pm 26$	$K_M = 369 \pm 62$ $K_m = 104 \pm 13$	$K_M = 301 \pm 10$ $K_m = 73 \pm 19$	$K_M = 218 \pm 17$ $K_m = 35 \pm 7$
Subject 3	$K_M = 201 \pm 39$ $K_m = 63 \pm 12$	$K_M = 219 \pm 29$ $K_m = 71 \pm 9$	$K_M = 201 \pm 32$ $K_m = 45 \pm 6$	$K_M = 180 \pm 19$ $K_m = 79 \pm 11$	$K_M = 173 \pm 19$ $K_m = 41 \pm 5$
Subject 4	$K_M = 185 \pm 16$ $K_m = 60 \pm 11$	$K_M = 393 \pm 25$ $K_m = 115 \pm 12$	$K_M = 378 \pm 51$ $K_m = 102 \pm 19$	$K_M = 230 \pm 18$ $K_m = 39 \pm 4$	$K_M = 235 \pm 47$ $K_m = 120 \pm 32$

K_M is the value of the maximum stiffness referred to the major axis.
K_m is the value of the minimum stiffness referred to the minor axis.

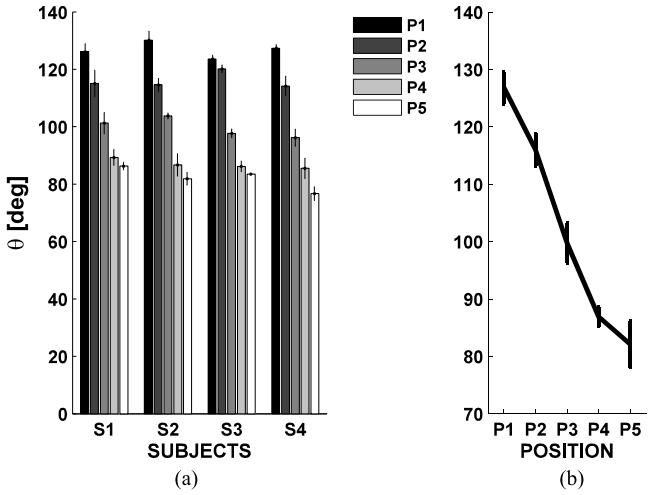

Fig. 16. (a) Mean values of the computed θ (deg) for each subject (S1, S2, S3, and S4) and position in the workspace. Different colors represent the five different position (P1, P2, P3, P4, and P5) of the workspace where the θ was estimated. Error bars represent $\pm$SD. (b) Mean values of the θ in the five different positions of evaluation (P1, P2, P3, P4, and P5), regardless subjects.

inertia. This tends to reduce in a significant way the bandwidth of the device, which is supposed to deliver a number of fast disturbances (force or position) in different directions, in order to estimate the directional properties of the human arm. Moreover, the use of a robotic manipulandum for estimating the arm stiffness is likely to conflict with the specific requirements of haptic rendering, which is indeed the focal aspect of many interactive tasks and the design criteria for most of such technologies. On the basis of the previous considerations, we decided to design a novel device for measuring endpoint stiffness with the following requirements to uncouple stiffness measurement from haptic rendering generated by the robot on which the device is plugged to maximize the operational speed and consequently minimizing the measurement time. The *cam-based* design described in this paper allows partly fulfilling the requirements above with a potential limitation due to the fast multidirectional perturbation that inevitably leads to vibrations and noise which could affect the accuracy of the measurements. Another important aspect which is worth to mention is that multiple perturbations over different directions involve also contribution by the stretch reflex in the final outcome. The proposed system demonstrated that it is possible to obtain reliable arm stiffness estimation in a reduced amount of time: the evaluated ellipses present shape and orientation values which have been found to be comparable with those obtained in previous works using the same procedure of multidirectional perturbations [13], [16], [18], [19], [20]. It is worth to mention that in some of the cited references, subjects were asked to relax muscles prior each directional perturbation, while in our study we wanted to test the reliability of the system when subject is voluntarily contracting muscles and check if the variability of the electromyography was negligible across execution time. As suggested by Figs. 13 and 15, the axes ratio and the orientation of the ellipses indicate a strong relation with the geometrical configuration of the human arm. The orientation of the major axis identifies the direction of highest stiffness for a certain configuration and the outcomes demonstrated that the major axis is always directed from the distal (wrist) to the proximal joint (shoulder) of the arm, as expected and showed in the cited researches. Furthermore, Fig. 16 highlights the difference in ellipse orientation across the five configurations of the human arm: ellipse orientation changes significantly among the different arm postures and the major axis results always directed from the distal to the proximal anatomical joint. A further behavior can be observed from Fig. 15 where the ratio between the axes is still dependent on arm posture but much more variable across subjects: in fact, if for the orientation of the major axis all the subjects presents similarities passing from positions 1 to 5, the dimension and ratio of the axes of the ellipse are highly dependent on several factors and subject anthropometry (i.e., level of muscular contraction and biomechanics of the muscular fibers which differ from subject to subject [40]). That is why if we can affirm that the proposed system provided results which are comparable with those in previous researches in terms of ellipse orientation, for what concern the dimension of the ellipse intersubject variability is extremely high; despite the stiffness values (length of the axes) differ among subjects, the results are reasonable and the magnitude of the stiffness is acceptable if compared with previous studies.

B. Importance of the Stretch Reflex

Although the paradigm for stiffness estimation by using directional perturbation has been designed to try to acquire only the contribution from the voluntary muscular activity, without including in the restoring force from the stretch reflex, we believe

that for a *quasi-online* stiffness measurement during a human–robot interaction all the contributions by the CNS must be included and opportunely processed. Furthermore, since the device has been prevalently design having in mind a final application in rehabilitation robotic and assessment of motor recovery, the emergence of improvement in stiffness modulation during therapy must consider all the aspects related to voluntary and involuntary responses by the CNS, and the presence of the stretch reflex is one of them [47]–[49]. Furthermore, the presented outcomes have shown that the device is characterized by an intrinsic simplicity and allows studying human–robot interaction without the need of implementing additional controllers on the robotic devices on which the system is plugged. The greatest achievement is the possibility to obtain the stiffness estimation within a single trial, overcoming the problem related to the intertrial variability which was present in the previously cited works, or using the simple mechanics of the system the number of perturbations can be arbitrarily chosen: i.e., if a single directional perturbation is requested, it will be sufficient to rotate the *cam* by a position controller and achieving much higher linear velocity values at the end-effector than the ones obtained by the use of a planar robotic device. Even if 960 ms of execution time, still cannot be referred as an online estimation of muscular stiffness, in robotic rehabilitation, the dynamics of movement are relatively slow and considering that the device applies 4 mm planar radial displacements, the subject's motion during robot therapy would not be dramatically disrupted. The possibility of getting information on the patient's capacity to modulate his/her muscular stiffness can provide unprecedented insights on motor recovery processes which are not anymore solely based on kinematics and force/torque acquisition but more on a measurement of the strategy of interaction with the environment.

C. Future Perspective in Human–Robot Interaction

Another important aspect arising from having a *quasi-online* measurement of endpoint stiffness is related to the emerging interest in the field of human-centered robotics [50]–[52] involving the close interaction between robotic systems and human beings, or even surgical robotics [53], [54] and robotic rehabilitation [55], [56]. The question arises as to whether is possible to have a continuous information of the muscular stiffness geometry of the biological counterpart during manipulation, in order to implement a robust controller able to adapt and to regulate the physical interaction at the interface between the robot and the human. It is clear that all the information about endpoint stiffness must be obtained with noninvasive methods in order not to alter the interaction between the human and the robot to be controlled; there are several on-going researches using techniques from high frequency vibro-inertial measurements [57] and time–frequency approach using haptic assistance [58] to gather information of the arm dynamics, to real-time parametric stiffness observer using variable stiffness actuation [59], [60] devices, which are able to provide information on force/displacement and measurements perceived at the interface between the human and the robotic device. A promising technique for online stiffness identification focuses on the analysis of EMG signals [61]–[63] by limiting the use of any actuated mechanism and to obtain information on human interaction: the common feature among all the EMG-based technique is the need of having a mathematical model describing the dynamic of the limb which is obtained by an initial calibration between arm force and electromyography, in order to obtain a reliable estimation of the stiffness ellipse. The hardware proposed in this paper, despite presenting intrinsic limitations in bandwidth and quasi-online stiffness estimation, does not need any *a priori* hypothesis and information about the subject or precalibration and aims at providing the experimenter or the clinician with a ready-for-use interface to measure and characterize arm stiffness in human–robot interaction and more precisely in robotic rehabilitation.

ACKNOWLEDGMENT

The work has carried out by a collaboration between Nanyang Technological University, Singapore and the Fondazione Istituto Italiano di Tecnologia, Genoa, Italy. The authors would like to thank Prof. P. Morasso and Prof. V. Sanguineti for the fundamental contributions to the research.

REFERENCES

[1] D. Rancourt and N. Hogan, "Dynamics of pushing," *J. Motor Behav.*, vol. 33, no. 4, pp. 351–362, 2001.
[2] A. Bicchi, S. L. Rizzini, and G. Tonietti, "Compliant design for intrinsic safety: General issues and preliminary design," in *Proc. IEEE/RSJ Int. Conf. Intell. Robots Syst.*, 2001, pp. 1864–1869.
[3] R. L'Orsa, C. J. Macnab, and M. Tavakoli, "Introduction to haptics for neurosurgeons," *Neurosurgery*, vol. 72, no. Suppl. 1, pp. 139–53, Jan. 2013.
[4] M. Tavakoli, R. V. Patel, and M. Moallem, "Haptic interaction in robot-assisted endoscopic surgery: A sensorized end-effector," *Int. J. Med. Robot.*, vol. 1, no. 2, pp. 53–63, Jan. 2005.
[5] K. Kim, J. E. Colgate, J. J. Santos-Munne, A. Makhlin, and M. A. Peshkin, "On the design of miniature haptic devices for upper extremity prosthetics," *IEEE/ASME Trans. Mechatronics*, vol. 15, no. 1, pp. 27–39, Feb. 2010.
[6] J. E. Colgate and N. Hogan, "Robust control of dynamically interacting systems," *Int. J. Control*, vol. 48, pp. 65–88, 1988.
[7] N. Hogan, "The mechanics of multi-joint posture and movement control," *Biol. Cybern.*, vol. 52, pp. 315–331, 1985.
[8] T. Flash and I. Gurevich, "Models of motor adaptation and impedance control in human arm movements," in *Self-Organization, Computational Maps, and Motor Control Volume 119*, P. G. Morasso and V. Sanguineti, Eds. Amsterdam, The Netherlands: Elsevier-Science, 1997, pp. 423–481.
[9] M. Darainy, N. Malfait, P. L. Gribble, F. Towhidkhah, and D. J. Ostry, "Learning to control arm stiffness under static conditions," *J. Neurophysiol.*, vol. 92, no. 6, pp. 3344–3350, Dec. 2004.
[10] A. G. Feldman, "Functional tuning of nervous system with control of movement or maintenance of a steady posture. III. Mechanographic analysis of the execution by man of the simplest motor tasks," *Biofzika*, vol. 11, pp. 667–675, 1966.
[11] D. T. Westwick and E. J. Perreault, "Closed-loop identification: Application to the estimation of limb impedance in a compliant environment," *IEEE Trans. Biomed. Eng.*, vol. 58, no. 3, pp. 521–530, Mar. 2011.
[12] J. M. Dolan, M. B. Friedman, and M. L. Nagurka, "Dynamic and loaded impedance components in the maintenance of human arm posture," *IEEE Trans. Syst., Man, Cybern.*, vol. 23, no. 3, pp. 698–709, May/Jun. 1993.
[13] F.A. Mussa-Ivaldi, N. Hogan, and E. Bizzi, "Neural, mechanical, and geometric factors subserving arm posture in humans," *J. Neurosci.*, vol. 5, pp. 2732–2743, 1985.
[14] R. Shadmehr, F. A. Mussa-Ivaldi, and E. Bizzi, "Postural force fields of the human arm and their role in generating multijoint movements," *J. Neurosci.*, vol. 13, pp. 45–62, 1993.
[15] J. McIntyre, F. A. Mussa-Ivaldi, and E. Bizzi, "The control of stable arm postures in the multi-joint arm," *Exp. Brain Res.*, vol. 110, pp. 62–73, 1996.
[16] T. Tsuji, P. Morasso, K. Goto, and K. Ito, "Human hand impedance characteristics during maintained posture in multi-joint arm movements," *Biol. Cybern.*, vol. 72, pp. 475–485, 1995.

[17] J. M. Dolan, M. B. Friedman, and M. L. Nagurka, "A testbed for measurement of human arm impedance parameters," in *Proc. IEEE Conf. Syst. Eng.*, 1990, pp. 123–126.

[18] E. Burdet, R. Osu, D. W. Franklin, T. E. Milner, and M. Kawato, "A method for measuring hand stiffness during multi-joint arm movements," *J. Biomech.*, vol. 33, pp. 1705–1709, 2000.

[19] H. Gomi and M. Kawato, "Equilibrium-point control hypothesis examined by measured arm stiffness during multijoint movement," *Science*, vol. 272, no. 5258, pp. 117–120, 1996.

[20] H. Gomi and M. Kawato, "Human arm stiffness and equilibrium-point trajectory during multijoint movement," *Biol. Cybern.*, vol. 76, pp. 163–171, 1997.

[21] D. J. Bennett, "Torques generated at the human elbow joint in response to constant position errors imposed during voluntary movements," *Exp. Brain Res.*, vol. 95, pp. 488–498, 1993.

[22] D. J. Bennett, J. M. Hollerbach, Y. Xu, and I. W. Hunter, "Time-varying stiffness of human elbow joint during cyclic voluntary movement," *Exp. Brain Res.*, vol. 88, pp. 433–442, 1992.

[23] F. Lacquaniti, M. Carrozzo, and N. A. Borghese, "Time-varying mechanical behavior of multijointed arm in man," *J. Neurophysiol.*, vol. 69, pp. 1443–1464, 1993.

[24] E. J. Perreault, R. F. Kirsch, and A. M. Acosta, "Multiple-input, multiple-output system identification for the characterization of limb stiffness dynamics," *Biol. Cybern.*, vol. 80, pp. 327–337, 1999.

[25] D. J. Bennett, M. Gorassini, and A. Prochazka, "Catching a ball: Contributions of intrinsic muscle stiffness, reflexes, and higher order responses," *Can. J. Physiol. Pharmacol.*, vol. 72, no. 5, pp. 525–534, May 1994.

[26] E. De Vlugt, F. C. T. Van der Helm, and A. C. Schouten, "Adaptation of reflexive feedback during arm posture to different environments," *Biol. Cybern.*, vol. 87, pp. 10–26, 2002.

[27] P. H. Chang and S. H. Kang, "Stochastic estimation of human arm impedance under nonlinear friction in robot joints: A model study," *J. Neurosci. Methods*, vol. 189, no. 1, pp. 97–112, May 30, 2010.

[28] M. Iwasaki, T. Shibata, and N. Matsui, "Disturbance-observer-based nonlinear friction compensation in table drive system," *IEEE/ASME Trans. Mechatronics*, vol. 4, no. 1, pp. 3–8, Mar. 1999.

[29] S. H. Scott, "Apparatus for measuring and perturbing shoulder and elbow joint positions and torques during reaching," *J. Neurosci. Methods*, vol. 89, no. 2, pp. 119–127, Jul. 15, 1999.

[30] A. M. Acosta, R. F. Kirsch, and E. J. Perreault, "A robotic manipulator for the characterization of two-dimensional dynamic stiffness using stochastic displacement perturbations," *J. Neurosci. Methods*, vol. 102, pp. 177–186, 2000.

[31] I. S. Howard, J. N. Ingram, and D. M. Wolpert, "A modular planar robotic manipulandum with end-point torque control," *J. Neurosci. Methods*, vol. 181, no. 2, pp. 199–211, Jul. 30, 2009.

[32] L. Masia, V. Squeri, G. Sandini, and P. Morasso, "Measuring end-point stiffness by means of a modular mechatronic system," in *Proc. IEEE Int. Conf. Robot. Autom.*, May 14–18, 2012, pp. 2471–2478.

[33] L. Masia, G. Sandini, and P. Morasso, "Preliminary design of a novel system for estimating end-point stiffness," in *Proc. Annu. Int. Conf. IEEE Eng. Med. Biol. Soc.*, Aug. 30–Sep. 3, 2011, pp. 8170–8174.

[34] L. Masia, G. Sandini, and P. G. Morasso, "A novel mechatronic system for measuring end-point stiffness: Mechanical design and preliminary tests," in *Proc. IEEE Int. Conf. Rehabil. Robot.*, Jun. 29–Jul. 1, 2011, pp. 1–6.

[35] Y. Qiu, D. J. Perreault, T. A. Keim, and J. G. Kassakian, "Nonlinear system modeling, optimal cam design, and advanced system control for an electromechanical engine valve drive," *IEEE/ASME Trans. Mechatronics*, vol. 17, no. 6, pp. 1098–1110, Dec. 2012.

[36] M. A. Krutky, V. J. Ravichandran, R. D. Trumbower, and E. J. Perreault, "Interactions between limb and environmental mechanics influence stretch reflex sensitivity in the human arm," *J. Neurophysiol.*, vol. 103, no. 1, pp. 429–440, 2010.

[37] J. A. Pruszynski, I. Kurtzer, and S. H. Scott, "The long-latency reflex is composed of at least two functionally independent processes," *J. Neurophysiol.*, vol. 106, no. 1, pp. 449–459, 2011.

[38] C. Capaday, R. Forget, R. Fraser, and Y. Lamarre, "Evidence for a contribution of the motor cortex to the long-latency stretch reflex of the human thumb," *J. Physiol.*, vol. 440, pp. 243–255, 1991.

[39] F. Doemges and P. M. H. Rack, "Changes in the stretch reflex of the human first dorsal interosseous muscle during different tasks," *J. Physiol.*, vol. 447, pp. 563–573, 1992.

[40] H. Patel, G. O'Neill, and P. Artemiadis, "On the effect of muscular co-contraction on the 3d human arm impedance," *IEEE Trans. Biomed. Eng.*, vol. 61, no. 10, pp. 2602–2608, Oct. 2014.

[41] G. N. Lewis, E. J. Perreault, and C. D. Mackinnon, "The influence of perturbation duration and velocity on the long-latency response to stretch in the biceps muscle," *Exp. Brain Res.*, vol. 163, pp. 361–369, 2005.

[42] K. S. Maluf, B. K. Barry, Z. A. Riley, and R. M. Enoka, "Reflex responsiveness of a human hand muscle when controlling isometric force and joint position," *Clin. Neurophysiol.*, vol. 118, pp. 2063–2071, 2007.

[43] L.-Q. Zhang and W. Z. Rymer, "Simultaneous and nonlinear identification of mechanical and reflex properties of human elbow joint muscles," *IEEE Trans. Biomed. Eng.*, vol. 44, no. 12, pp. 1192–1209, Dec. 1997.

[44] D. G. Asatryan and A. G. Feldman, "Functional tuning of the nervous system with control of movements or maintenance of a steady posture," *Biophysics*, vol. 10, pp. 925–935, 1965.

[45] A. G. Feldman and A. F. Levin, "The origin and use of positional frames of reference in motor control," *Behav. Brain Sci.*, vol. 18, pp. 723–806, 1995.

[46] E. Bizzi, A. Polit, and P. Morasso, "Mechanisms underlying achievement of final position," *J. Neurophysiol.*, vol. 39, pp. 435–444, 1976.

[47] R. D. Trumbower, V. J. Ravichandran, M. A. Krutky, and E. J. Perreault, "Altered multijoint reflex coordination is indicative of motor impairment level following stroke," in *Proc. IEEE Conf. Eng. Med. Biol. Soc.*, vol. 2008, 2008, pp. 3558–3561.

[48] C. G. Meskers, A. C. Schouten, J. H. de Groot *et al.*, "Muscle weakness and lack of reflex gain adaptation predominate during post-stroke posture control of the wrist," *J. Neuroeng. Rehabil.*, vol. 6, p. 29, ISSN: 1743-0003, 2009.

[49] F. W. Cody, C. N. Goodwin, and H. C. Richardson, "Effects of ischaemia upon reflex electromyographic responses evoked by stretch and vibration in human wrist flexor muscles," *J. Physiol.*, vol. 391, pp. 589–609, Oct. 1987.

[50] M. Grebenstein and P. van der Smagt, "Antagonism for a highly anthropomorphic hand–arm system," *Adv. Robot.*, vol. 22, pp. 39–55, 2008.

[51] M. Zinn, O. Khatib, B. Roth, and J. K. Salisbury, "Playing it safe," *IEEE Robot. Autom. Mag.*, vol. 11, no. 2, pp. 12–21, Jun. 2004.

[52] D. Mitrovic, S. Klanke, and S. Vijayakumar, "Learning impedance control of antagonistic systems based on stochastic optimization principles," *Int. J. Robot. Res.*, vol. 30, no. 2, pp. 1–18, 2011.

[53] M. T. Perri, A. L. Trejos, M. D. Naish, R. V. Patel, and R. A. Malthaner, "Initial evaluation of a tactile/kinesthetic force feedback system for minimally invasive tumor localization," *IEEE/ASME Trans. Mechatronics*, vol. 15, no. 6, pp. 925–931, Dec. 2010.

[54] M. Piccigallo, U. Scarfogliero, C. Quaglia, G. Petroni, P. Valdastri, A. Menciassi, and P. Dario, "Design of a novel bimanual robotic system for single-port laparoscopy," *IEEE/ASME Trans. Mechatronics*, vol. 15, no. 6, pp. 871–878, Dec. 2010.

[55] A. Gupta and M. K. O'Malley, "Design of a haptic arm exoskeleton for training and rehabilitation," *IEEE/ASME Trans. Mechatronics*, vol. 11, no. 3, pp. 280–289, Jun. 2006.

[56] R. Riener, L. Lunenburger, S. Jezernik, M. Anderschitz, G. Colombo, and V. Dietz, "Patient-cooperative strategies for robot-aided treadmill training: First experimental results," *IEEE Trans. Neural Syst. Rehabil. Eng.*, vol. 10, no. 3, pp. 380–394, Sep. 2005.

[57] H. M. Hondori and W. T. Ang, "Smart mug to measure hand's geometrical mechanical impedance," in *Proc. Annu. Int. Conf. IEEE Eng. Med. Biol. Soc.*, Aug. 30-Sep. 3, 2011, pp. 4053–4056.

[58] D. Piovesan, P. Morasso, P. Giannoni, and M. Casadio, "Arm stiffness during assisted movement after stroke: The influence of visual feedback and training," *IEEE Trans. Neural Syst. Rehabil. Eng.*, vol. 21, no. 3, pp. 454–465, May 2013.

[59] G. Grioli and A. Bicchi, "A real-time parametric stiffness observer for VSA devices," in *Proc. IEEE Int. Conf. Robot. Autom.*, May 9–13, 2011, pp. 5535–5540.

[60] G. Grioli and A. Bicchi, "A non-invasive real-time method for measuring variable stiffness," presented at the Robotics: Science and Systems, Zaragoza, Spain, Jun. 2010.

[61] W. Gallagher, D. Gao, and J. Ueda, "Improved stability of haptic human–robot interfaces using measurement of human arm stiffness," *Adv. Robot.*, vol. 28, no. 13, pp. 869–882, 2014.

[62] J. Rosen, M. Brand, M. Fuchs, and M. Arcan, "A myosignal-based powered exoskeleton system," *IEEE Trans. Syst., Man, Cybern. A, Syst., Humans*, vol. 32, no. 3, pp. 210–222, May 2001.

[63] H. K. Kim, B. Kang, B. Kim, and S. Park, "Estimation of multijoint stiffness using electromyogram and artificial neural network," *IEEE Trans. Syst., Man, Cybern. A: Syst., Humans*, vol. 39, no. 5, pp. 972–980, Sep. 2009.

L. Masia (M'07) graduated in mechanical engineering from the "Sapienza" University of Rome, Roma, Italy, in 2003, and received the Ph.D. degree in mechanical measurement for engineering from the University of Padua, Padova, Italy, in 2007.

During his Ph.D. degree, he was a Visiting Student in the Mechanical Engineering Department, Massachusetts Institute of Technology (from January 2005 to December 2006) working at the Newman Lab for Biomechanics and Human Rehabilitation under the supervision of Dr. Hermano Igo Krebs and Prof. NevilleHogan. He held a TeamLeader position at the Italian Institute of Technology leading the Motor Learning and Rehabilitation Laboratory of the Robotics Brain and Cognitive Sciences Department from February 2007 to July 2013. He is currently an Assistant Professor in the School of Mechanical and Aerospace Engineering, Nanyang Technological University, Singapore. His research is mainly focused on design and development of novel mechatronic devices for rehabilitation and implementation of control strategies for human–robot interaction.

V. Squeri received the Bachelor and Master degrees in biomedical engineering from the University of Genova, Genova, Italy, in 2004 and 2006, respectively, with a thesis concerning the analysis of upper limb movements in patients affected by hemiparesis and the development and assessment of a robot therapy rehabilitation protocol for patients with multiple sclerosis. Under the supervision of Prof. Pietro Morasso, she received the Ph.D. degree in humanoid technologies from the Italian Institute of Technology and University of Genova in 2010. Her project focused on using a planar robotic manipulandum to study sensorimotor adaptation and promote neuromotor recovery.

She currently has a Postdoctoral position at the Italian Institute of Technology. She is focusing her research on the development of new robotic treatments that aim to promote functional and motor recovery. In particular, the main activities will be the implementation and validation of exercises for the assessment and training of proprioceptive and motor impairments in children and adults affected by neurological disorders (i.e., celebral palsy, oncological trauma, ataxia and stroke, multiple sclerosis).